

# Coupled CSD/CFD non-linear aeroelastic trim of HiReNASD wing in transonic regime

(Received: Sep 24, 2016. Revised: Oct 26, 2016. Accepted: Jan 27, 2017)

G. ROMANELLI<sup>1,\*</sup>  
P. MANTEGAZZA<sup>1</sup>

## Abstract

The present work is aimed at assessing the credibility of a multi-fidelity aeroservoelastic analysis toolbox by tackling a set of static aeroservoelastic problems and comparing the results with reference experimental and numerical data available in literature. The availability of such an integrated environment is almost mandatory from the very beginning of the design process. More in particular we investigate the sensitivity to different modelling options for representing the aerodynamic sub-system. In such a way it is easier to strike the best balance between accuracy of the results and computational efficiency, choosing within the hierarchy of tools available the lowest-fidelity Doublet Lattice Method (DLM) or the Non-Linear Full Potential (NLFP) equations or the Euler equations or the highest-fidelity Reynolds Averaged Navier-Stokes (RANS) equations.

More in particular the static aeroelastic benchmark test problem of computing the reference equilibrium or “trim” configuration of the HiReNASD wing is presented. Such an example is of particular interest because it was selected as a benchmark test problem for the AIAA Aeroelastic Prediction Workshop series with the objective of providing an impartial forum for assessing state-of-the-art Computational Aeroelasticity (CA) methods as practical tools for the prediction of static and dynamic aeroservoelastic phenomena within the transonic regime. More precisely, after providing an overview of the structural and aerodynamic models, we compute the static aeroelastic response of the wing in attached axes by means of the iterative method and compare the results with reference experimental data. Such a procedure is repeated for different angles of attack  $\alpha \in (-1.5^\circ, 4.5^\circ)$  in order to highlight the non-linear phenomena associated with the transonic regime.

## 1. Introduction

The aeroservoelastic interaction between aerodynamic, elastic and control forces tends to dominate the behavior of modern, highly flexible, aeronautical structures, as a consequence of the weight savings and efficiency improvements resulting from e.g. multidisciplinary optimization procedures, extensive use of composite materials. Therefore the availability of an integrated environment for aeroservoelastic analysis is almost mandatory from the very beginning of the design process. [11]

The coupling of dedicated state-of-the-art fluid and structure solvers for aeroelastic analysis is a well established research topic. Together with the availability of more and more powerful computing resources, current trends pursue the adoption of high fidelity mathematical models and numerical methods, e.g. Computational Structural Dynamics (CSD) or Multibody System Dynamics (MSD) for the structural sub-system and Computational Fluid Dynamics (CFD) for the aerodynamic sub-system. [4, 3] This choice is somehow obliged when dealing with non-linear aeroelastic phenomena, such as in the transonic regime (typical cruise condition of modern aircraft) where sub/supersonic regions are simultaneously present within the flow-field and we observe a complex interaction e.g. between the shock waves and the structural displacements. [15] A better understanding of these phenomena is important to design more efficient and safer aircraft. In fact the accuracy of the classical, computationally efficient,

<sup>1</sup> Politecnico di Milano, Department of Aerospace Sciences and Technologies, via La Masa 32, 20100, Milano, IT

\* Corresponding author. Email: [romanelli@aero.polimi.it](mailto:romanelli@aero.polimi.it)

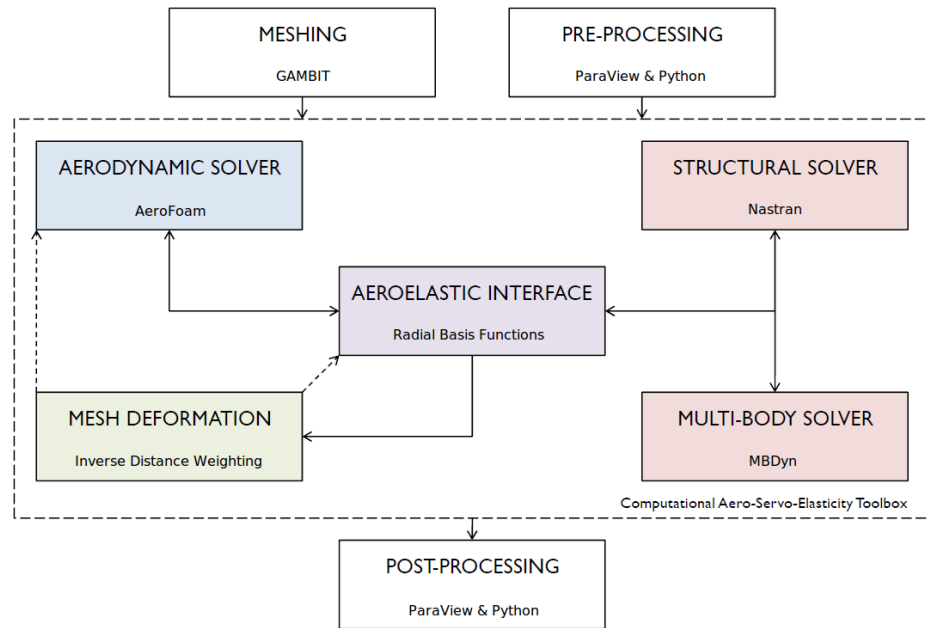


**Figure 1:** Architecture of proposed high-fidelity aeroservoelastic analysis toolbox.

linearized numerical methods for aeroelastic analysis is significantly reduced as the Mach number increases. Therefore the present trend in the aerospace industry, even in preliminar design, is that of replacing or better placing side by side such low-fidelity methods with high-fidelity more expensive ones. [6]

The objective of the present work is to illustrate the numerical results of an in-house implemented toolbox for solving intrinsically multidisciplinary non-linear Fluid-Structure Interaction (FSI) problems with a partitioned approach, that is coupling high-fidelity CSD and CFD tools by means of a robust, flexible aeroelastic interface scheme. With reference to Figure 1, the architecture of the toolbox can be summarized as follows: the aeroelastic interface provides all the functionalities to link the key Finite Element (FE) structural solver Nastran with the Finite Volume (FV) aerodynamic solver AeroFoam. Moreover for dealing with moving boundary problems in Arbitrary Lagrangian Eulerian (ALE) formulation a dedicated mesh deformation tool is available. [7]

As benchmark test case we tackle the problem of computing the reference equilibrium or “trim” configuration of the HiReNASD wing. Such an example is of particular interest because it was selected as a benchmark test problem for the AIAA Aeroelastic Prediction Workshop series. More in particular we investigate the sensitivity to different modelling options for representing the aerodynamic sub-system, such as Non-Linear Full Potential, Euler and Reynolds Averaged Navier Stokes (RANS) equations (respectively within a density-based and pressure-based framework).

## 2. HiReNASD wing

Currently, a benchmarking standard for use in validating the accuracy of CA codes does not exist. Many aeroelastic data sets have been obtained in wind-tunnel and flight testing. However none have been globally recognized as an ideal data set. There are numerous reasons for this. One is that often such aeroelastic data sets focus on the aeroelastic phenomena alone (flutter, for example) and do not contain associated information, such as unsteady pressures or structural deflections. Other available data sets focus solely on the unsteady pressures. Other deficiencies include omission of relevant data, such as flutter frequency or the acquisition of qualitative deflection data. In addition to these content deficiencies, all of the available data sets present both experimental and computational technical challenges.

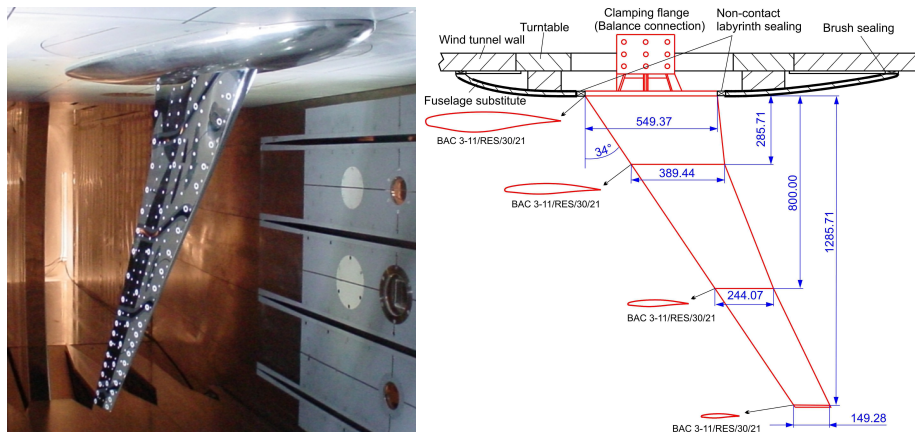


**Figure 2:** Experimental set-up for the HiReNASD wing.

Experimental issues include facility influences, non-linearities beyond those being modelled, and data post-processing. From a computational perspective, technical challenges include modelling geometric complexities, coupling between the flow and the structure, turbulence modelling, grid issues, and boundary conditions. Moreover the availability of suitable computational resources in order to yield feasible turn-around times for CA simulations should also be considered as a potential bottleneck. An Aeroelasticity Benchmark Assessment task was initiated at NASA in 2009 with the objectives of a) examining the existing potential experimental data sets and selecting the one(s) viewed as the most suitable for computational benchmarking and b) performing an initial computational evaluation of these configurations using the NASA in-house computational aeroelastic software as part of the code validation process.

A successful effort results in the identification of a focus problem for government, industry, and academia to use in demonstrating and comparing codes, methodologies, and experimental data to advance the state-of-the-art. Ideally such a focus problem would be the first of many put forth for this purpose, with a future goal being the design, fabrication, and testing of an aeroelastic model recognized by the community as a benchmark test case. Excellent examples of such a progression and escalation of code validation in the international community are the series of AIAA Drag Prediction and High Lift Prediction workshops. These workshops have three main objectives: a) to assess the ease and practicality of using state-of-the-art computational methods for aerodynamic load prediction, b) to impartially evaluate the effectiveness of the high-fidelity solvers and c) to identify areas for improvement. The structure of such initiatives provides a template for other computational communities seeking similar improvements in accuracy within their own fields. The examination and selection of aeroelastic data sets within the Aeroelasticity Benchmark Assessment task together with the computational evaluation of these configurations led to initiation of an AIAA Aeroelastic Prediction Workshop series.

The High Reynolds Number Aero-Structural Dynamics (HiReNASD) project was led by Aachen University with funding from the German Research Foundation (DFG). It was initiated in 2004 to produce a high-quality transonic aeroelastic data set at realistic flight Reynolds numbers for a large transport-type wing/body configuration and tested in the European Transonic Windtunnel (ETW) in 2006. This experiment was selected among the benchmark test problems for the AIAA Aeroelastic Prediction Workshop series kick-off. [5]

The HiReNASD experimental set-up shown in Figure 2 is a ceiling-mounted, semi-span, clean-wing configuration with a leading-edge sweep angle  $\Lambda_{LE} = 34^\circ$ , a span  $b = 1.2857$  m and a mean aerodynamic chord  $\bar{c} = 0.3445$  m. It consists of three sections. The two outboard sections use an 11-percent thick BAC3-11/RES/30/21 supercritical airfoil. The inboard section uses the same airfoil thickened linearly from 11-percent at its outer edge to 15-percent at

the root. To minimize boundary layer interference during testing, a generic fuselage was included, mechanically isolated from the wing by a labyrinth seal. Extensive measurements were acquired during testing of the HiReNASD model. Instrumentation included a six-component balance, Surface Pattern Tracking (SPT) optical markers for surface deformation measurements on the pressure side of the wing, 11 accelerometers, 28 strain-gages, and 259 unsteady pressure transducers. The pressure transducers were distributed along the upper and lower surfaces at 7 span sections.

The HiReNASD test matrix consisted of both static and dynamic measurements at different flow conditions, with Reynolds number  $Re$  varying from  $7 \cdot 10^6$  up to  $73 \cdot 10^6$  and dynamic pressures up to  $q_\infty = 130 \cdot 10^3$  Pa at the following transonic Mach numbers  $M_\infty \in (0.70, 0.75, 0.80, 0.83, 0.85, 0.88)$ . The test medium was nitrogen. For static testing, pressure distribution and lift and drag coefficients were acquired at different angles of attack. Dynamic testing involved forced vibrations of the wing at the natural frequencies of the first bending, second bending, and first torsion modes and was performed over the range of Reynolds numbers at different angles of attack.

The objective of the present work is that of comparing (in terms of aerodynamic loads and structural displacements) the numerical results of the multi-fidelity toolbox for aeroservoelastic analysis `AeroFoam` with the experimental data of run No. 132 of the HiReNASD project, corresponding to the static aeroelastic response of the wing/body at Reynolds number  $Re = 7 \cdot 10^6$ , Mach number  $M_\infty = 0.8$  and dynamic pressure  $q_\infty = 40055$  Pa and choosing the following angles of attack  $\alpha \in (-1.5^\circ, 0.0^\circ, 1.5^\circ, 3.0^\circ, 4.5^\circ)$ .

### 3. Structural model

In literature the choice of the appropriate structural model is quite controversial. In fact two different Finite Element (FE) are available from the HiReNASD project website. Both are based on a very detailed discretization of the wing/body structure in uniform solid elements, tetrahedral or hexahedral respectively, for more than 200000 grid points. The two models yield slightly different modal frequencies with differences below 5% and the first 8 dynamically relevant modal shapes are almost identical.

However the current trend within the framework of AIAA Aeroelastic Prediction Workshop series is that of choosing a Finite Element (FE) stick beam structural model with limited d.o.f. and successively tuning e.g. the material properties in order to match as closely as possible the natural frequencies and modal shapes measured experimentally by means of Ground Vibration Test (GVT). With reference to Table 1 and Figure 1 we choose a FE stick beam structural model with only 62 nodes, each connected with 4 additional nodes (at leading edge, trailing edge, maximum and minimum thickness locations within each  $x - z$  section of the wing/body) by means of rigid elements for a total of  $N_s = 310$  grid points. The addition of such extra nodes is beneficial for assembling the aeroelastic interface operator as it makes possible to use only translation d.o.f. but at the same time accurately reconstruct rotations.

**Table 1:** Modal bases used for the non-linear aeroelastic trim analysis of HiReNASD wing.

Mode	Frequency $f$ [Hz]	Description
1	25.95	1 <sup>st</sup> bending
2	82.42	2 <sup>nd</sup> bending
3	117.58	1 <sup>st</sup> in-plane bending
4	168.42	1 <sup>st</sup> bending-torsion
5	258.38	3 <sup>rd</sup> bending
6	273.20	4 <sup>h</sup> bending
7	275.29	2 <sup>nd</sup> in-plane bending
8	275.29	2 <sup>nd</sup> bending-torsion

It is worthwhile to remark that both the wing and the fuselage are modelled as deformable structures: such a choice is beneficial in terms of robustness of the mesh deformation algorithm. [5]

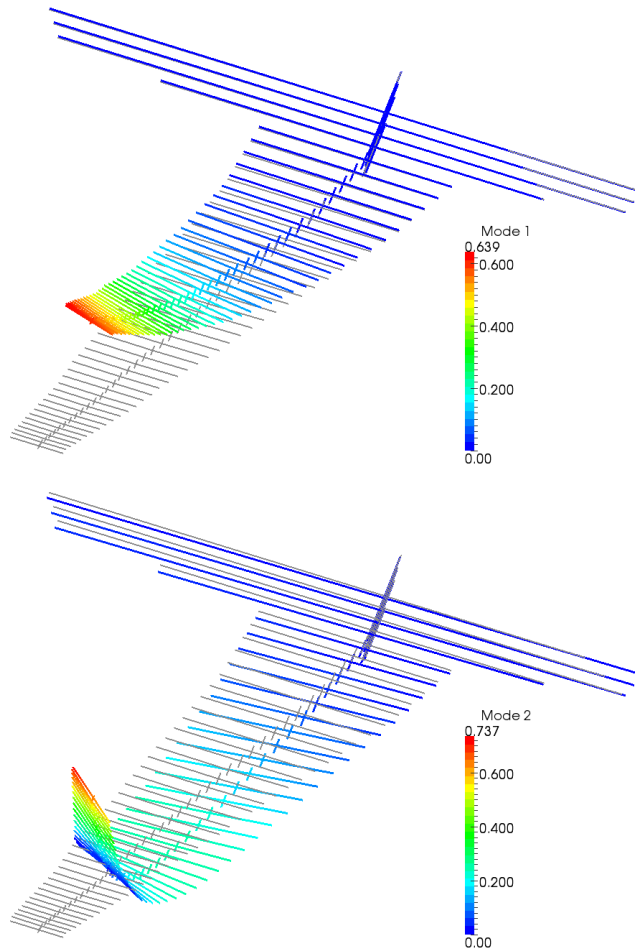


**Figure 3:** Stick beam FE structural model of the HiReNASD wing deformed according to first and second attached modal shapes.

#### 4. Aerodynamic model

To tackle the aerodynamic problem a wide hierarchy of mathematical models and numerical methods of increasing fidelity but also computational cost is available. Since the very large number of simulations to be accounted for to complete even a simple aeroelastic assessment, a classical choice is to pick the computationally efficient, linearized numerical methods to evaluate the unsteady aerodynamic loads due to the structural displacements. However when dealing with non-linear transonic aerodynamics it is advisable to resort to the more sophisticated tools offered by CFD.

More in particular the objective is that of performing a comparison between the numerical results of Non-Linear Full Potential (NLFP), Euler and Reynolds Averaged Navier Stokes (RANS) simulations. To this end we resort to the following analysis tools:

- A two-field, node-centered, coupled solver for the NLFP equations, featuring linear/quadratic shape functions for space discretization operators and first/second order accurate time integration schemes. Unsteady entropy correction and embedded wake generation are also available. Moreover it implements a strategy for handling wake conditions without creating a dedicated boundary patch. For more details refer to [10].

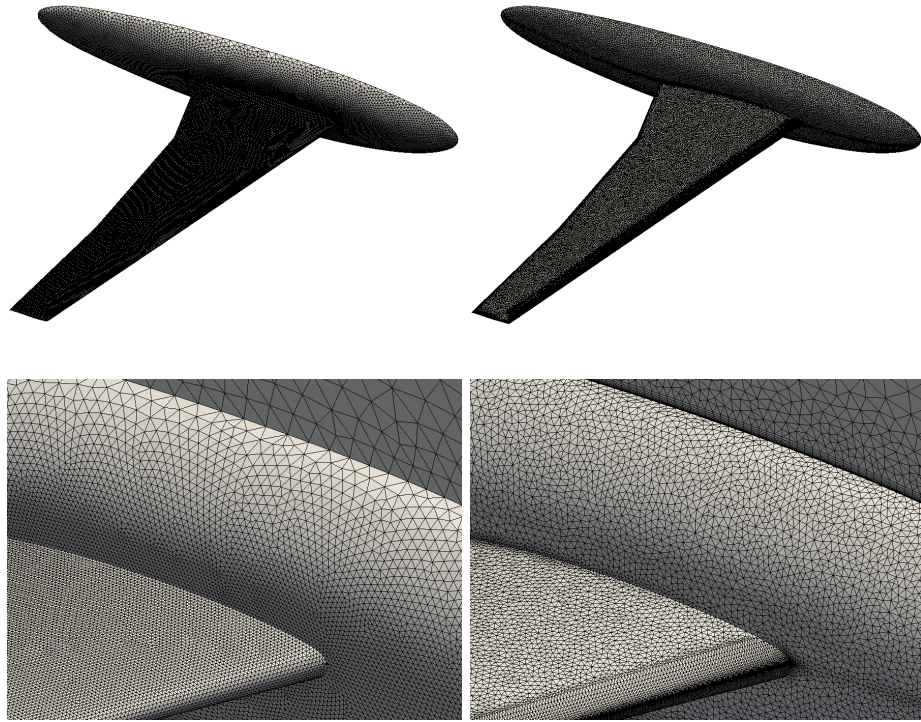


**Figure 4:** Surface aerodynamic meshes (with detailed view at wing-fuselage connection) for the HiReNASD wing for Euler (left) and RANS (right) simulations. In this latter case it is possible to appreciate the higher resolution and the prismatic boundary layer.

- A density-based, conservative-variables, cell-centered, coupled solver for the Euler/RANS equations, featuring second order accurate Approximate Riemann Solver (ARS) by Roe for inviscid fluxes space discretization and fully implicit first/second order accurate time integration schemes. For steady-state simulations Full-Multi-Grid (FMG) and Residual Smoothing (RS) convergence acceleration techniques are implemented. For more details refer to [14, 13, 12].
- A pressure-based, primitive variables, cell-centered, segregated solver for the RANS equations, implementing a pressure correction approach and the so-called SIMPLE-C strategy for pressure-velocity coupling, suitable for calculating steady-state flows at all speeds. High resolution is implemented by means of a deferred approach for improved numerical stability. For more details refer to [1, 8].

To quantify the computational effort, for all inviscid (NLFP and Euler) runs we use an aerodynamic mesh with  $N_{a,b} = 136130$  boundary faces and  $N_{a,v} = 963719$  tetrahedral cells while for all viscous (RANS) runs we use an aerodynamic mesh with  $N_{a,b} = 176474$  boundary faces and  $N_{a,v} = 1909304$  hybrid tetrahedral and hexahedral (within the boundary layer and wake regions) cells as shown in Figure 4. We adopt the Spalart-Allmaras turbulence model popular within the aeronautical industry with the density-based RANS solver.

Decomposing the problem on 16 Intel Xeon X5650 processors, a non-linear aeroelastic trim simulation converges with residuals below  $\epsilon \leq 10^{-3}$  in 2 and 8 hours for Euler and RANS simulations respectively.

## 5. Mesh deformation

Once the structural displacements and velocities are suitably interpolated by means of the aeroelastic interface operator as illustrated in [12], it is necessary to tackle the problem of adjusting the internal aerodynamic mesh to the newly computed boundary nodes in such a way that grid quality is not degraded significantly, e.g. with non-negative cell volumes, moderate levels of stretching and non-orthogonality. This task of moving what can amount up to millions of

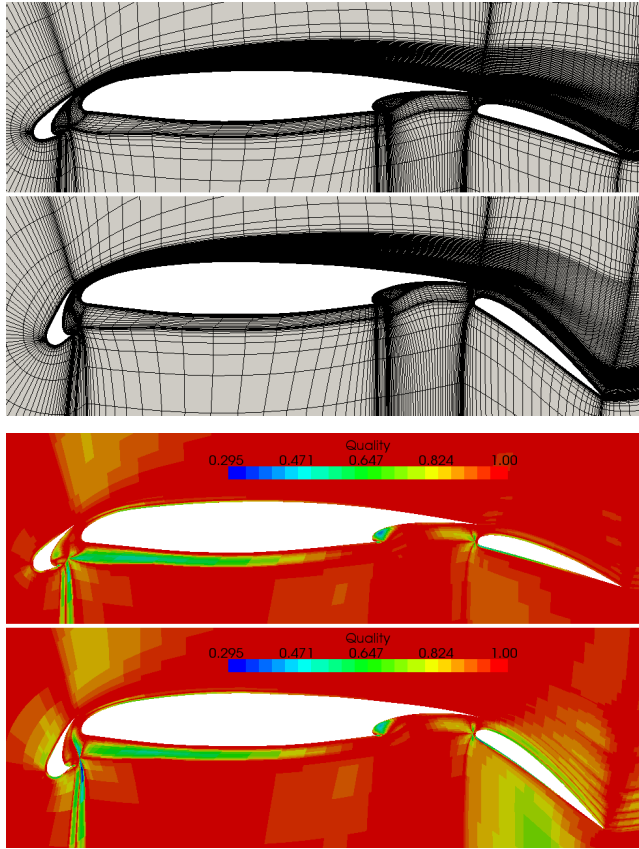


**Figure 5:** Aileron and slat rotation with  $\delta = 20^\circ$  applied to the structured hexahedral anisotropic mesh of a multi-element airfoil (left). The cell-wise normalized Jacobian mesh quality measure shows only a moderate deterioration (right).

nodes is to be performed thousand of times during an aeroservoelastic computation. Therefore the availability of efficient, massively parallel and robust mesh deformation tools and topology modifiers is crucial. [9, 4, 2, 17]

In order to achieve the best compromise between the opposing requirements of accuracy, robustness and (parallel) efficiency we propose a hierarchical mesh deformation strategy, based on a modified version of the Inverse Distance Weighting (IDW) multivariate interpolation kernel

Rather than using algorithms that require solving a system of equations (expensive in terms of computational cost and memory occupation for realistic simulations), we choose an explicit mesh deformation technique based on the Inverse Distance Weighting (IDW) multivariate interpolation scheme. For each  $k$ -th internal d.o.f. the displacement  $\Delta \mathbf{x}_k$  relative to the reference undeformed configuration  $\mathbf{x}_k$  can be evaluated by performing the following matrix-array multiplication:

$$\Delta \mathbf{x}_k = \sum_{j=0}^{N_{a,b}} \frac{\mathbf{IDW}_{(k,j)}}{|\mathbf{IDW}_{(k,:)}|} \mathbf{s}_j \quad \forall \quad k = [1, N_a, v], \quad (1)$$

with the interpolation kernel  $\mathbf{IDW}_{(k,j)} = \|\mathbf{x}_k - \mathbf{x}_j\|^{-p}$ . The parameter  $p$  can be used as a knob to adjust the size of the computational stencil and therefore the smoothness of the results. As it is, this strategy can be either time-efficient or memory-efficient, depending on whether matrix  $\mathbf{IDW}$  is computed only once in the pre-processing stage and then stored with a large memory overhead. In order to achieve the best trade-off we propose a simple and effective modification to the original interpolation algorithm called Sparse Inverse Distance Weighting (SIDW) in which matrix  $\mathbf{IDW}$  is stored in Compressed Sparse Column (CSC) format as follows:

$$\mathbf{SIDW}_{(k,j)} = \mathbf{IDW}_{(k,j)} \quad \text{if} \quad \frac{\mathbf{IDW}_{(k,j)}}{|\mathbf{IDW}_{(k,:)}|} > \xi \quad (2)$$

where  $\xi$  is a threshold parameter to be set by the user. This is somehow similar to modified Sheperd's method but it is simpler to implement since it does not require any fast spatial search structure. [16] The computational cost and memory requirements can be estimated as  $\mathcal{O}(cN_{a,v})$ , where  $c \ll N_{a,b}$  is the average number of active columns. This method is very powerful also because it does not require any knowledge of the connectivity of the mesh and it is suited for a straightforward parallelization as it is not susceptible to implementation issues such as in the case of shared nodes among many processors.

The two-dimensional benchmark test problem shown in Figure 5-6 is concerned with the deformation of a structured hexahedral anisotropic mesh of a multi-element airfoil subject to a rigid rotation of both slat and flap control surfaces up to  $\delta \geq 30^\circ$ . Such an example is of particular interest because for meshes with very high levels of stretching classical mesh deformation algorithms, e.g. laplacian smoothing, suffer a sudden and significant drop in quality and robustness. This drawback is only albeit mitigated by choosing ad hoc diffusivity functions, e.g. quadratic. On the contrary the proposed algorithm is not affected by such issues. With reference to Figure 5 it is possible to appreciate the small changes in the contours of the cell-wise normalized Jacobian mesh quality measure, especially near-by the slat and flap control surfaces and with peak value at the slat leading edge.

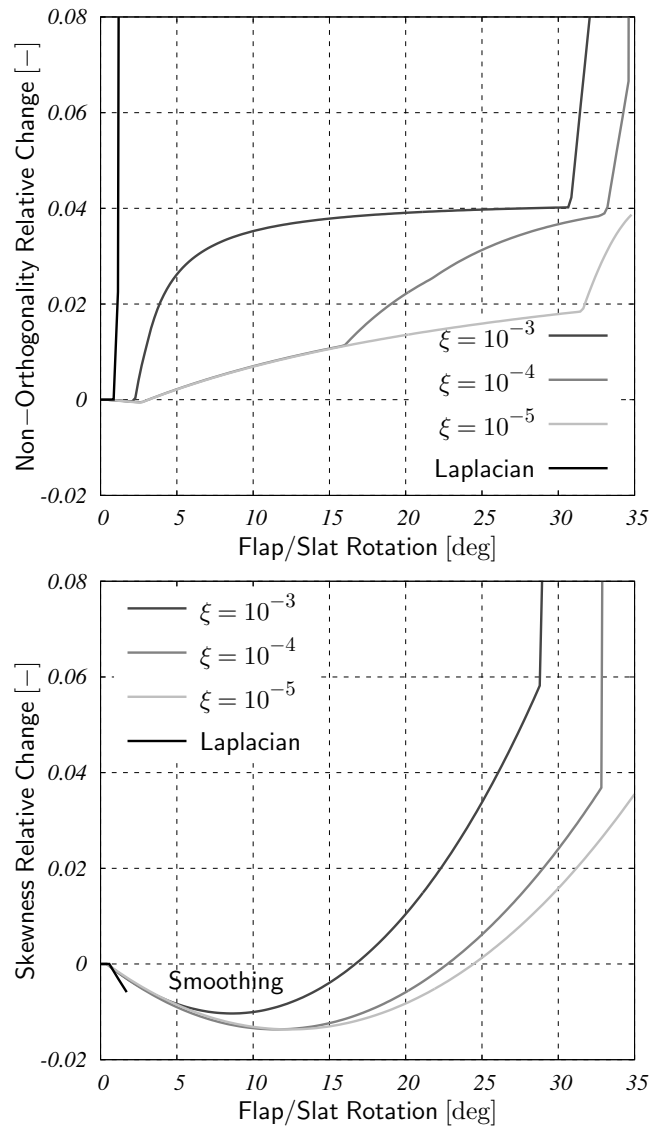
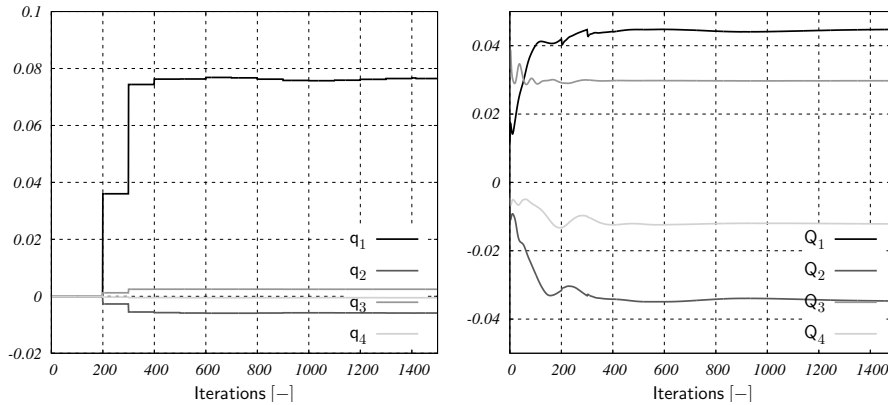


**Figure 6:** Relative changes in cell-wise non-orthogonality (top) and skewness (bottom) mesh quality measures as a function of slat/flap rotation angle with  $p = 2$  and tuning knob  $\xi$ .

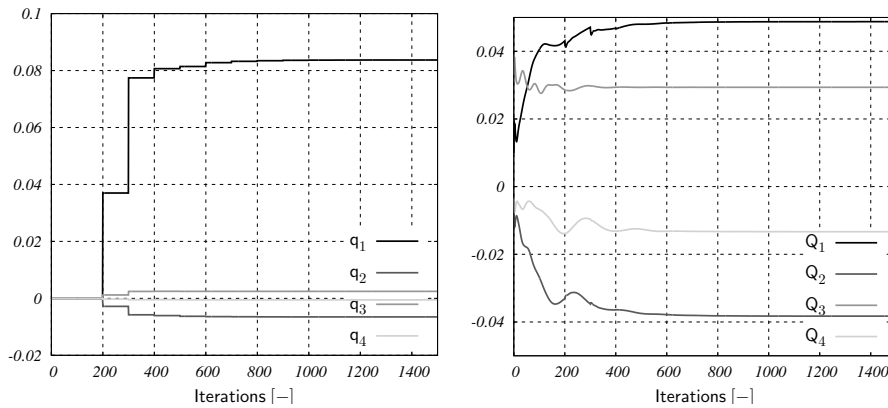
## 6. Trim analysis

Two types of static aeroelastic simulation can be carried out, i.e. restrained and free-flying. For the case of a wind tunnel model attached to the wind tunnel wall, the case is called a restrained case. The attachment provides the balancing forces and moments according to the aerodynamic and inertial loads working on the model. The modelling of such a problem in static aeroelastic simulations is straightforward.

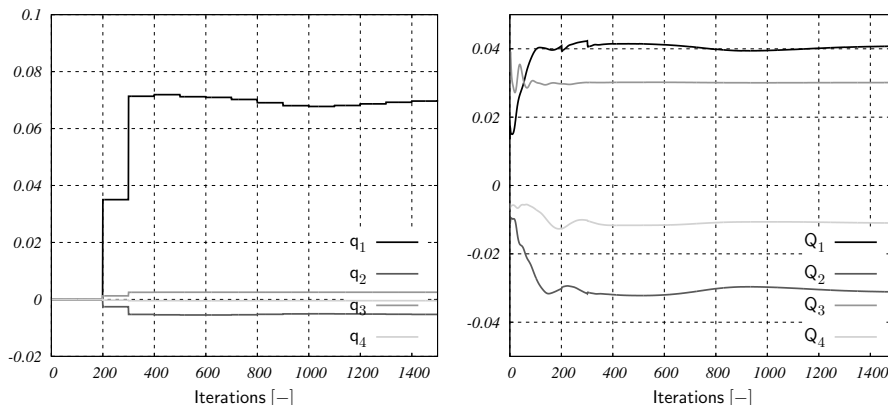
At each  $k$ -th outer iteration the Generalized Aerodynamic Forces (GAF) are computed and the classical iterative method is solved for the corresponding generalized displacements. These steps are repeated until convergence to the non-linear trim of an elastic aircraft.



**Figure 7:** Convergence history of the generalized displacements (left) and the generalized aerodynamic forces (right) for NLFP for  $\alpha = 1.5^\circ$ .

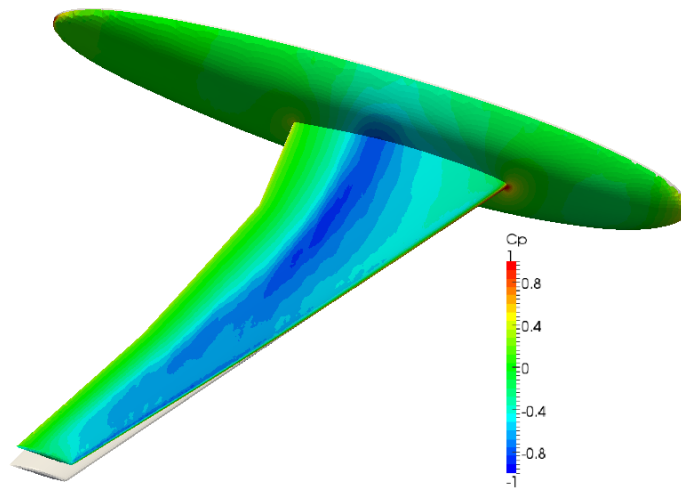


**Figure 8:** Convergence history of the generalized displacements (left) and the generalized aerodynamic forces (right) for Euler for  $\alpha = 1.5^\circ$ .

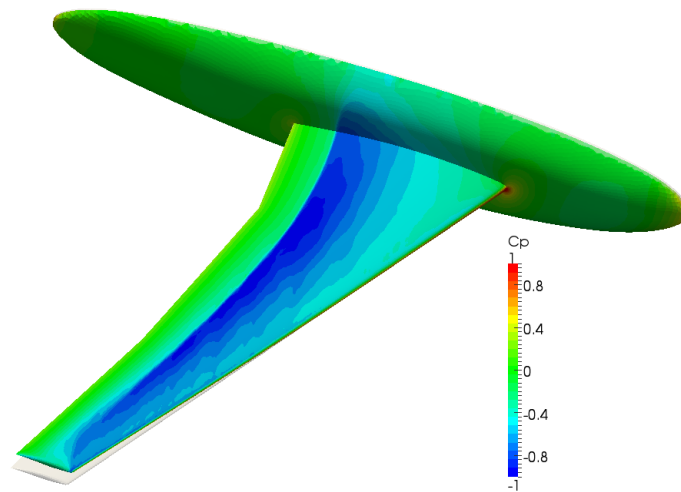


**Figure 9:** Convergence history of the generalized displacements (left) and the generalized aerodynamic forces (right) for RANS for  $\alpha = 1.5^\circ$ .

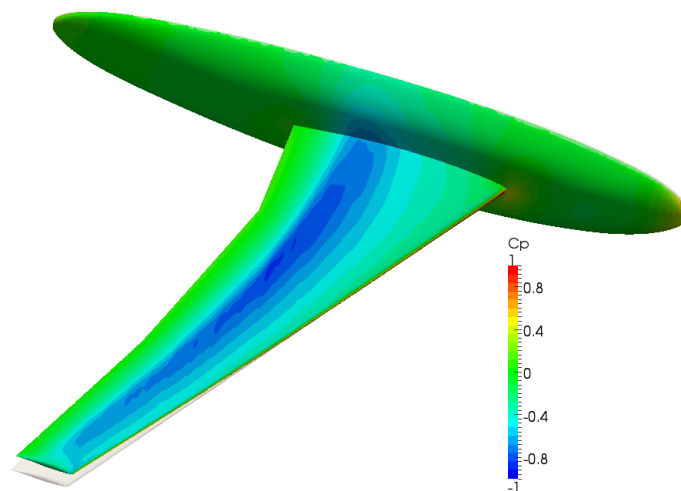
**Figure 10:** Pressure coefficient  $C_p$  contours for  $\alpha = 1.5^\circ$  on the deformed configuration ( $5\times$  magnified) predicted by NLFP model.



**Figure 11:** Pressure coefficient  $C_p$  contours for  $\alpha = 1.5^\circ$  on the deformed configuration ( $5\times$  magnified) predicted by Euler model.



**Figure 12:** Pressure coefficient  $C_p$  contours for  $\alpha = 1.5^\circ$  on the deformed configuration ( $5\times$  magnified) predicted by RANS model.



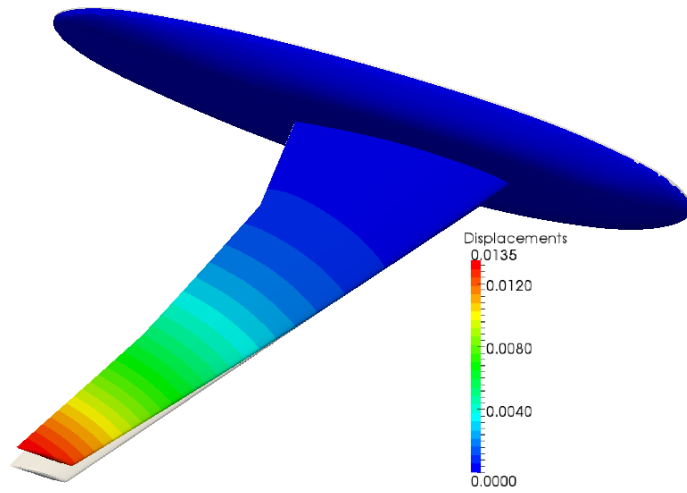


**Figure 13:** Structural displacements  $|\mathbf{s}|$  contours for  $\alpha = 1.5^\circ$  on the deformed configuration ( $5\times$  magnified) predicted by NLFP model.

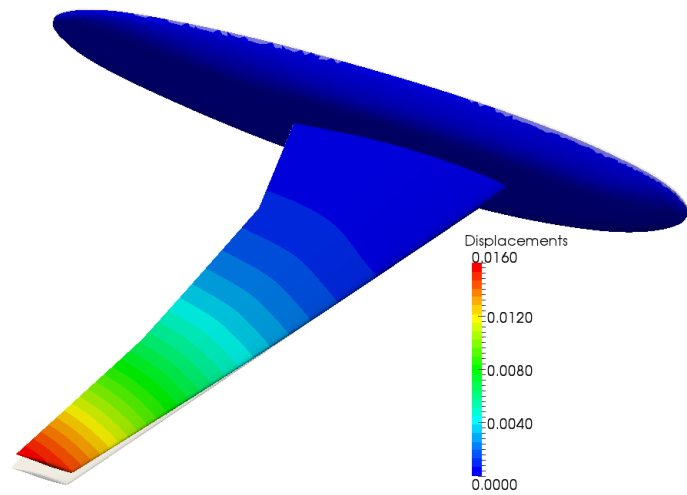


**Figure 14:** Structural displacements  $|\mathbf{s}|$  contours for  $\alpha = 1.5^\circ$  on the deformed configuration ( $5\times$  magnified) predicted by Euler model.

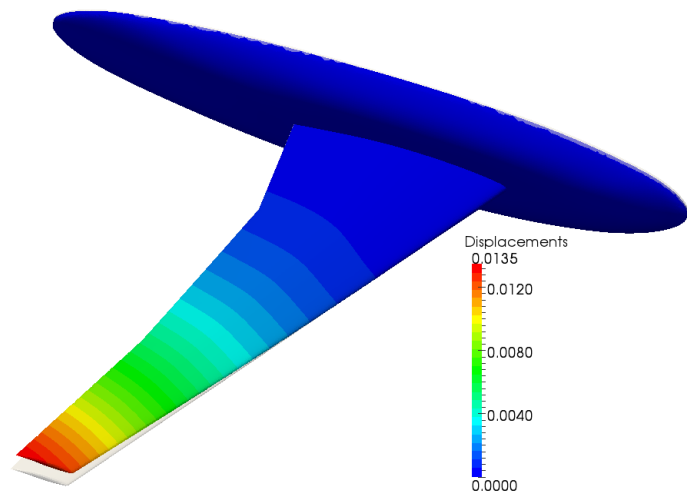


**Figure 15:** Structural displacements  $|\mathbf{s}|$  contours for  $\alpha = 1.5^\circ$  on the deformed configuration ( $5\times$  magnified) predicted by RANS model.

In Figures 7-9 the convergence history of the elastic d.o.f. and of the generalized aerodynamic forces is shown for NLFP, Euler and RANS simulations for  $\alpha = 1.5^\circ$ . After a first block of 200 inner iterations to start-up the non-linear aeroelastic trim procedure the elastic d.o.f are updated with a relaxation factor  $\omega = 0.5$  until convergence within a suitable tolerance  $\epsilon = 10^{-4}$  in less than 3000 inner iterations. It is interesting to remark that the Euler simulation converges monotonically to larger generalized displacements than the RANS simulation. In this latter case it is also necessary to increase the number of inner iterations to drive the residuals below the same threshold.

In Figures 10-15 the contours of the pressure coefficient  $C_p$  and the structural displacements  $|\mathbf{s}|$  are shown onto the final configuration of the wing/body with elastic deformations suitably magnified for  $\alpha = 1.5^\circ$ . It is possible to qualitatively appreciate the stronger expansion of the flow on the upper surface of the wing and the corresponding sharper shock wave for the Euler simulation with respect to RANS, e.g. because of the absence of diffusive phenomena. Viceversa the numerical results of NLFP simulation are affected by a significantly higher level of numerical dissipation, thus leading to a more smeared shock wave and lower wing loading.

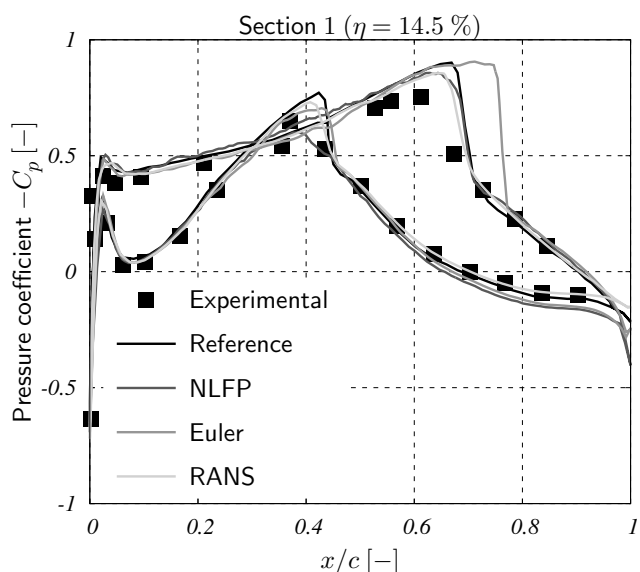


**Figure 16:** Comparison of the distribution of the pressure coefficient  $C_p$  between experimental data and NLFP, Euler and RANS on Section 1.

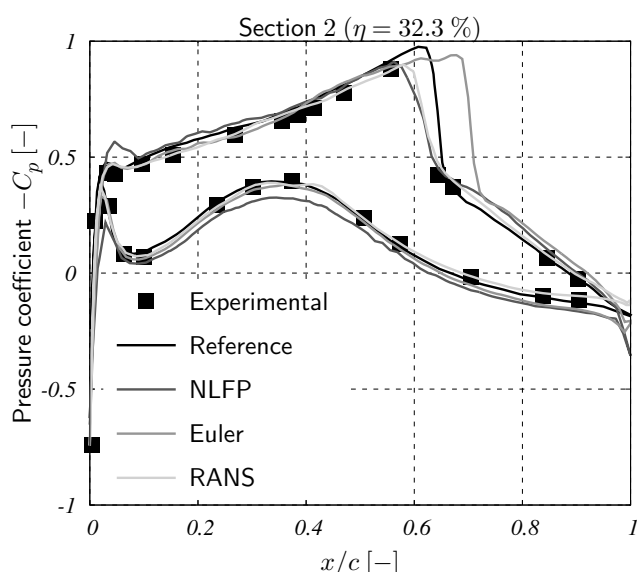


**Figure 17:** Comparison of the distribution of the pressure coefficient  $C_p$  between experimental data and NLFP, Euler and RANS on Section 2.

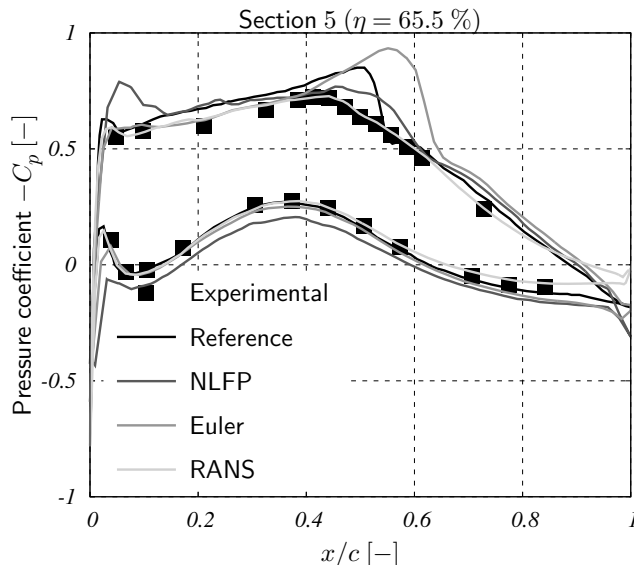


**Figure 18:** Comparison of the distribution of the pressure coefficient  $C_p$  between experimental data and NLFP, Euler and RANS on Section 5.

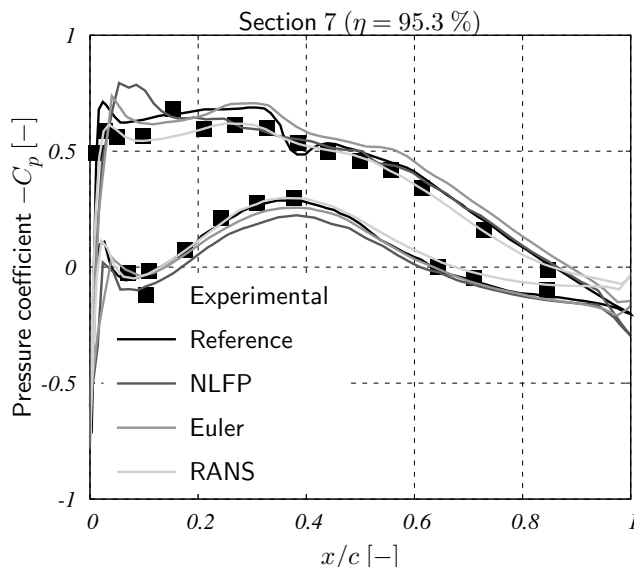


**Figure 19:** Comparison of the distribution of the pressure coefficient  $C_p$  between experimental data and NLFP, Euler and RANS on Section 7.

As a result the aerodynamic loads and therefore the structural displacements are larger for the Euler simulation with respect to RANS. More quantitative results can be found in Figure 16-19 with a comparison of the distribution of the pressure coefficient  $C_p$  along reference wing sections between NLFP, Euler and RANS simulations and experimental data for  $\alpha = 1.5^\circ$ . It is interesting to remark that the numerical results of RANS simulation fairly agree with the reference experimental and numerical data. Viceversa the numerical results of Euler simulation show a 5% shift downstream of the shock wave position and therefore a significant increment of the aerodynamic loads. The numerical results of NLFP should converge to those of Euler simulation. However they fall quite close to the experimental data because of the numerical dissipation of the NLFP solver here selected. [10] Finally in Figure ?? the maximum wing tip displacements are plotted as a function of the angle of attack  $\alpha$  together with the relative errors with respect to the experimental data. It is worthwhile to remark that the relative errors associated with RANS is significantly lower than those associated with NLFP or Euler for  $\alpha \leq 3.0^\circ$ . Viceversa for  $\alpha = 4.5^\circ$  the accuracy of NLFP, Euler and RANS predictions are comparable.

**Figure 20:** Maximum wing tip displacement as a function of angle of attack  $\alpha$  or NLFP, Euler and RANS simulations.

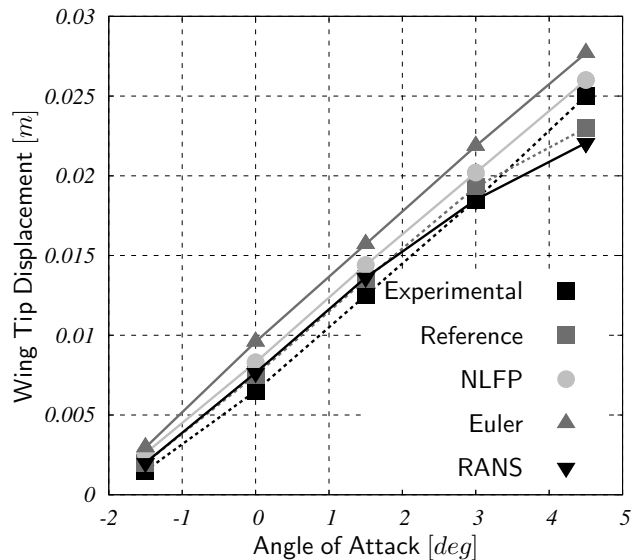
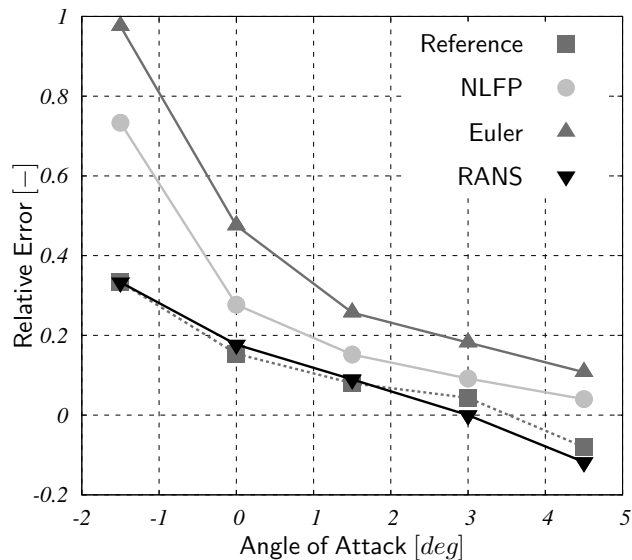


**Figure 21:** Relative error with respect to experiments (right) for NLFP, Euler and RANS simulations.



## 7. Conclusions

In the present work we assessed the credibility of a multi-fidelity aeroservoelastic analysis toolbox, built coupling high-fidelity CSD and CFD tools, by tackling the static aeroelastic benchmark test problem of computing the reference equilibrium or trimmed configuration of the HiReNASD wing and comparing the results with reference experimental and numerical data available in literature. Such an example is of particular interest because it was selected as a benchmark test problem for the AIAA Aeroelastic Prediction Workshop.

More in particular we investigated the sensitivity to different modeling options for representing the aerodynamic sub-system. In such a way it is easier to strike the best balance between accuracy of the results and computational efficiency, choosing within the hierarchy of tools available the Non-Linear Full Potential (NLFP) equations or the Euler equations or the Reynolds Averaged Navier-Stokes (RANS) equations. In general there is a good agreement with reference experimental data, especially at lower angle of attacks, while at higher angles of attack RANS simulations tend to predict a non-linear behavior.

## References

- [1] J. Blazek. *Computational Fluid Dynamics: Principles and Applications*. Oxford University Press, 2001.
- [2] F. Bos. “Moving and Deforming Meshes for Fapping Fight at Low Reynolds Numbers”. *5-th OpenFOAM Workshop*, 2005.
- [3] L. Cavagna, P. Masarati, and G. Quaranta. “Coupled Multibody/CFD Simulation of Maneuvering Flexible Aircraft”. *Journal of Aircraft*, Vol. 48, No. 1, 2011.
- [4] L. Cavagna, G. Quaranta, G. L. Ghiringhelli, and P. Mantegazza. “Efficient Application of CFD Aeroelastic Methods Using Commercial Software”. *International Forum on Aeroelasticity and Structural Dynamics*, 2005.
- [5] P. Chwalowski, J. P. Florance, J. Heeg, C. D. Wieseman, and B. Perry. “Preliminary Computational Analysis of the HiReNASD Configuration in Preparation for the Aeroelastic Prediction Workshop”. *International Forum on Aeroelasticity and Structural Dynamics*, 2011.
- [6] M. J. de C. Henshaw, K. J. Badcock, G. A. Vio, C. B. Allen, J. Chamberlain, I. Kaynes, G. Dimitriadis, J. E. Cooper, M. A. Woodgate, A. M. Rampurawala, D. Jones, C. Fenwick, A. L. Gaitonde, M. A. Taylor, D. S. Amor, T. A. Eccles, and C. J. Denley. “Non-linear Aeroelastic Prediction for Aircraft Applications”. *Progress in Aerospace Sciences*, 2007.
- [7] C. Farhat, P. Geuzaine, and C. Grandmon. “The Discrete Geometric Conservation Law and the Nonlinear Stability of ALE Schemes for the Solution of Flow Problems on Moving Grids”. *Journal of Computational Physics*, Vol. 174, 2001.
- [8] R. J. Hirsch. *Numerical Computation of Internal & External Flows*. Wiley, 1989.
- [9] H. Jasak. “Dynamic Mesh Handling in OpenFOAM”. *47-th AIAA Aerospace Sciences Meeting*, 2009.
- [10] A. Parrinello and P. Mantegazza. “Independent Two-Fields Solution for Full-Potential Unsteady Transonic Flows”. *AIAA Journal*, Vol. 48, No. 7, 2010.
- [11] M. Patil and D. Hodges. “Flight Dynamics of Highly Flexible Flying Wings”. *Journal of Aircraft*, Vol. 43, No. 6, 2006.
- [12] G. Romanelli, M. Castellani, and S. Ricci. “Coupled CSD/CFD Non-Linear Aeroelastic Trim of Free-Flying Flexible Aircraft”. *53-rd AIAA/ASME/ASCE Structures, Structural Dynamics and Materials Conference*, 2012.
- [13] G. Romanelli and L. Mangani. “Object-Oriented Redesign of Density-Based RANS Solver AeroFoam for Aerodynamic/Aeroelastic Industrial Applications”. *5-th OpenCFD Conference*, 2010.
- [14] G. Romanelli, E. Serioli, and P. Mantegazza. “A Free Approach to Modern Computational Aeroelasticity”. *48-th AIAA Aerospace Sciences Meeting*, 2009.
- [15] D. M. Schuster, D. D. Liu, and L. J. Huttzell. “Computational Aeroelasticity: Success, Progress, Challenge”. *Journal of Aircraft*, Vol. 40, No. 5, 2003.

- [16] D. Shepard. “A Two-Dimensional Interpolation Function for Irregularly-Spaced Data”. *ACM National Conference*, 1968.
- [17] J. Witteveen. “Explicit Mesh Deformation Using Inverse Distance Weighting Interpolation”. *47-th AIAA Aerospace Sciences Meeting*, 2009.